reaction is moderately fast, equilibrium should be reached at our conditions if the reaction were only slightly exoergic. It thus appears that Reaction (7) must be at least 3 or 4 kcal/mole exoergic, which suggests that $\Delta H_f(HC_2O_4^+) \approx 60$ kcal/mole.

ACKNOWLEDGMENTS

The authors wish to express their appreciation for the financial support of The Robert A. Welch Foundation and also to Project SQUID of the Office of Naval Research, Department of the Navy, for the use of the instrument that was constructed with its support under Contract N0014-67-A0226-005, NR098-038.

* Present address: Burndy Corp., Richards Ave., Norwalk, Conn.

[1] J. H. Futrell and T. O. Tiernan, in *Fundamental Processes in Radiation Chemistry*, edited by P. Ausloos (Interscience, New York, 1968), Chap. 4, p. 171.
[2] S. M. Schildcrout and J. L. Franklin, J. Chem. Phys. **51,** 4055 (1969).
[3] T. W. Shannon and A. G. Harrison, J. Chem. Phys. **43,** 4201, 4206 (1965).
[4] A. G. Harrison and J. J. Myher, J. Chem. Phys. **46,** 3276 (1967).
[5] M. Saporoschenko and W. W. Wisner, Bull. Am. Phys. Soc. **13,** 206 (1968).
[6] Shuang-Ling Chong and J. L. Franklin, J. Chem. Phys. **54,** 1487 (1971).
[7] (a) J. B. Hasted, *Physics of Atomic Collisions* (Butterworths, Washington, D.C., 1969), p. 369; (b) p. 506.
[8] G. Gioumousis and D. P. Stevenson, J. Chem. Phys. **29,** 294 (1958).

THE JOURNAL OF CHEMICAL PHYSICS VOLUME 56, NUMBER 3 1 FEBRUARY 1972

Excitation Mechanisms of the Nitrogen First-Positive and First-Negative Radiation at High Temperature*

RICHARD C. FLAGAN AND JOHN P. APPLETON
Department of Mechanical Engineering, Massachusetts Institute of Technology, Cambridge, Massachusetts 02139

(Received 13 May 1971)

The kinetic mechanisms responsible for the excitation of the first-positive and first-negative emission of nitrogen have been investigated in a re-examination of previously reported shock-tube measurements of the nonequilibrium radiation for these systems. The rate coefficients of the collisional quenching reactions,

$$N_2(A\,^3\Sigma_u^+) + N(^4S) \xrightarrow{k_{-2}^{(N)}} N_2(X\,^1\Sigma_g^+) + N(^4S)$$

and

$$N_2^+(B\,^2\Sigma_u^+) + N_2(X\,^1\Sigma_g^+) \xrightarrow{k_q^{(N_2)}} N_2^+(X\,^2\Sigma_g^+) \quad \text{or} \quad N_2^+(A\,^2\Pi_u) + N_2(X\,^1\Sigma_g^+)$$

were found to be given by the empirical expressions, $k_{-2}^{(N)} = 5.1\times10^{-3}T^{-2.23}$ cm^3 sec^{-1} and $k_q^{(N_2)} = 1.9\times10^{-2}\,T^{-2.33}$ cm^3 sec^{-1}, respectively, over the approximate temperature range 6000–14 000°K.

I. INTRODUCTION

The characteristic nonequilibrium radiation profiles, which are observed in the relaxation region behind shock waves in nitrogen over the nominal wavelength intervals 6000–12 000 Å and 3500–5000 Å are generally attributed to the first-positive ($B\,^3\Pi_g \rightarrow A\,^3\Sigma_u^+$) and first-negative ($B\,^2\Sigma_u^+ \rightarrow X\,^2\Sigma_g^+$) band systems of N_2 and N_2^+, respectively, see Fig. 1.[1] The characteristic features of this nonequilibrium emission have been investigated by several authors.[2–14] Qualitatively, the radiation rises rapidly to a peak immediately after the shock wave, the peak intensity being far in excess of that which would correspond to complete thermochemical equilibrium and then decays in an exponentiallike fashion to the ultimate equilibrium level. The emitting states of the two band systems, i.e., $N_2(B\,^3\Pi_g)$ and $N_2^+(B\,^2\Sigma_u^+)$, are separated by more than 10 eV, and thus it is surprising that the times required to reach the peak intensity are quite comparable over a wide range of temperature,[13] typically 6000–15 000°K. This observation suggests common rate-limiting steps in the kinetic mechanisms which are responsible for populating both of the emitting states $N_2(B\,^3\Pi_g)$ and $N_2^+(B\,^2\Sigma_u^+)$.

In an attempt to examine the role of atomic nitrogen in shock-wave excitation mechanisms, Wray[12] observed the radiation behind shock waves passing through a nitrogen test gas which was already partially dissociated by means of a pulsed electrodeless discharge. Unfortunately, the initial atom concentrations in the test gas at the time when the shock waves passed the observation station were not accurately determined. The primary source of the inaccuracy appears to be that the low-temperature recombination rate coefficient which Wray used to estimate the atom concentration at the time of shock arrival was roughly a factor of 4 greater than the more recent and generally accepted value.[15–17] However, on the basis of Wray's measurements,[12] it is possible to conclude that nitrogen atoms are very much more effective in promoting collisional excitation of nitrogen molecules to both the $N_2(B\,^3\Pi_g)$ and

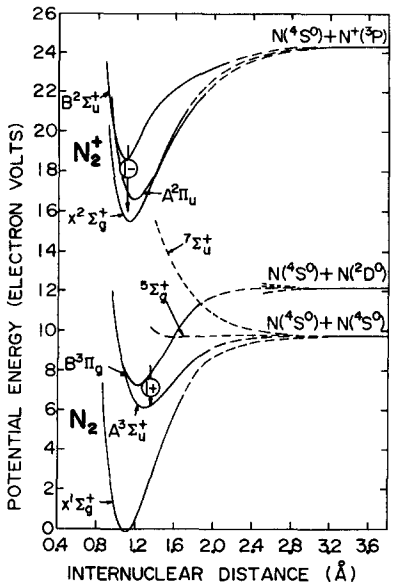

FIG. 1. Simplified potential-energy diagram of the N_2 molecule and N_2^+ ion from a more complete diagram of Gilmore.[1] The $N_2(1+)$ and $N_2^+(1-)$ emissions are indicated.

$N_2^+(B\,^2\Sigma_u^+)$ states than are the ground-state molecules $N_2(X\,^1\Sigma_g^+)$.

Marrone and Wurster[14] deduced rate constants for the excitation of the $N_2(A\,^3\Sigma_u^+)$ state by collisions of ground-state nitrogen with N, N_2, and e^- by matching observed times-to-peak intensity with times computed by integration of the flow conservation and chemical rate equations. The kinetic scheme used in that work omits the possible dissociation of $N_2(A\,^3\Sigma_u^+)$ which the present results indicate is a key factor in determining the absolute emission intensity of the $N_2(1+)$ band system.

Recent improvements in the understanding of the gas-phase dissociation and recombination kinetics of nitrogen, both experimentally[15–18] and theoretically,[19] prompted this re-examination of the role of atomic nitrogen in the excitation mechanisms which give rise to the first-positive and first-negative emission profiles observed behind shock waves. The investigation utilizes the measurements of the times to reach peak intensity and the radiation profile shapes which have been published in the literature,[2–12] together with some unpublished measurements, due to Wray,[13] of the times to reach peak intensity and the absolute emission intensities recorded in experiments where the test gas was not predissociated.

II. EXPERIMENTAL CONSIDERATIONS

A. Vibrational Relaxation

Figure 2 shows a plot of Wray's[13] measurements of the times, τ_{pk}, to reach peak intensity for both the $N_2(1+)$ and $N_2^+(1-)$ band systems as a function of the vibrationally relaxed but chemically frozen temperature. All of the experiments were conducted using undiluted nitrogen at an initial pressure of 1 torr. The full line in Fig. 2 shows the temperature variation of the characteristic vibrational relaxation time for ground-state N_2 as measured by Millikan and White[20] and Appleton.[21] It is clear from this comparison that the nitrogen gas was vibrationally relaxed well before the $N_2(1+)$ and $N_2^+(1-)$ radiation intensities had reached significant levels. For example, at $T=14\,000°K$ the induction time prior to the onset of dissociation is estimated to be 0.4 μsec using the diffusion theory of vibration–dissociation coupling of Brau, Keck, and Carrier.[22] This is roughly one-quarter the time to reach the peak intensity and is too short a time to be clearly resolved in the experimental measurements. At lower temperatures the induction time represents a smaller fraction of the time to peak. Thus, the initial post-shock temperatures were calculated using the Rankine–Hugoniot equations, and the assumption that the translational, rotational, and vibrational energy modes of the N_2 were fully equilibrated. However, with increasing distance behind the shock front, the temperature and pressure will vary due to both the dissociation of N_2 molecules and to the development of the cold wall boundary layer which acts as a mass sink for the shocked test gas.

B. Boundary Layer Effects

The effects of the shock-tube boundary layer on the properties of the shocked test gas have been investi-

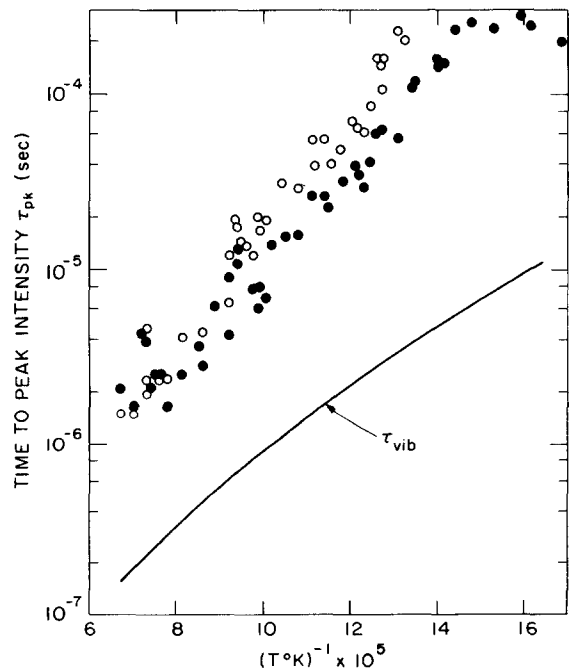

FIG. 2. Comparison of measured times-to-peak intensity due to Wray[13] ($P_1=1$ torr) and the characteristic vibrational relaxation time, τ_{vib}.[20,21] ●, $N_2(1+)$; ○, $N_2^+(1-)$; solid line, τ_v.

gated by numerous authors.[23–29] For this reason the subject will only be briefly considered here. Mirel's[28,29] treatment, which allows corrections to the ideal shock-tube flow properties due to boundary layer development, is the most widely quoted. The primary effect of the boundary layer growth in kinetic studies performed in small bore shock tubes at low initial pressures is to decrease the time of flight of a fluid element which passes through the shock wave at a fixed position upstream of the observation station below that calculated on the basis of ideal shock-tube theory. The corrections to the ideal flow properties are usually evaluated by assuming that at the observation station the shock and contact surface are traveling at the same speed, i.e., the mass leakage in the boundary layer which passes the contact surface is equal to the mass flux through the shock front. This condition was approximately satisfied in Wray's experiments. The mass continuity equation for the inviscid flow external to the boundary layer may then be written in the form

$$\rho u = \rho_2 u_2 [1-(x/l_m)^{1/2}], \tag{2.1}$$

where $\rho_2 u_2 = \rho_1 U_s$ is the mass flux entering the shock wave, x is the distance measured downstream from the shock wave in shock-fixed coordinates, and l_m is the maximum separation distance between the shock and the contact surface which is approached asymptotically and calculated as described by Mirels.[28] Since it is assumed that the shock waves travel at the uniform velocity U_s, then

$$x = U_s t_L, \tag{2.2}$$

where t_L is the laboratory observation time.

In order to analyze the chemically reacting flows obtained behind normal shock waves generated in a shock tube, a numerical computer program which uses a fourth-order Runga–Kutta integration technique to solve the simultaneous differential forms of the flow conservation equations together with the appropriate chemical rate equations, was developed. When viewed in shock-fixed coordinates, the flow is steady and is treated as being quasi-one-dimensional to account for the boundary layer mass loss as described by Eq. (2.1). The independent variable used in the analysis is x which is related to the actual particle flight time t_f by the equation,

$$dx/dt_f = u. \tag{2.3}$$

For a more detailed discussion of the calculation method, see the Appendix of Ref. 30.

C. Emission Intensity Calculation

Having determined the temperature, density, and species concentration histories in the relaxation region, the spectral band intensities of the radiation were calculated using the smeared rotational line model described by Keck, Camm, Kivel, and Wentink.[5] Thus, the spectral intensity I_λ is given as

$$I_\lambda = 2hc^2(\pi r_0)\, f[N]\langle\phi\rangle\lambda^{-5}(hc/kT)\, g''Q_r''Q_v''/g'Q_r'Q_v', \tag{2.4}$$

where $r_0 = e^2/mc^2$ is the classical electron radius, $f = |R(\bar{r})/ea_0|^2/3R_\infty\lambda$ is the absorption oscillator strength of the band system, and $|R(\bar{r})/ea_0|^2$ is the electronic transition moment dependent on the internuclear separation $\bar{r}$. The quantity ϕ is a dimensionless number of order unity which takes into account the details of the vibration–rotational spectrum, and the averaged quantity $\langle\phi\rangle$ is defined as

$$\langle\phi\rangle = \lambda^6 \int_{\lambda_1}^{\lambda_2} (\lambda')^{-6} R d\lambda' \Big/ \int_{\lambda_1}^{\lambda_2} R d\lambda', \tag{2.5}$$

where R is the experimentally determined resolution function of the optical instruments used in the experiments.[12] $[N']$ is the upper state concentration, and g', Q_r', and Q_v' are the corresponding electronic degeneracy, rotational, and vibrational partition functions, respectively, which were evaluated by assuming that the translational, rotational, and vibrational temperatures were equal (the double primes identify the corresponding absorbing state quantities).

In the calculations which were carried out for the purpose of comparison with Wray's[13] absolute intensity measurements, values for the electronic transition moments were those given by Wurster[31] for the $N_2(1+)$ system, i.e., $|R(\bar{r})/ea_0|^2 = 0.096$, and by Buttrey and McChesney[32] for the $N_2^+(1-)$ system, i.e., $|R(\bar{r})/ea_0|^2 = 0.45$.

III. KINETIC MODELS AND COMPUTATIONS

A. Reaction Mechanism: $N_2(1+)$

The kinetic scheme which was found to best describe the shock-tube measurements of the $N_2(1+)$ system is the following:

$$N_2(X\,{}^1\Sigma_g^+) + M \xrightarrow{k_{+1}^{(M)}} 2N({}^4S) + M, \tag{1}$$

$$N_2(X\,{}^1\Sigma_g^+) + N({}^4S) \underset{k_{-2}^{(N)}}{\overset{k_{+2}^{(N)}}{\rightleftharpoons}} N_2(A\,{}^3\Sigma_u^+) + N({}^4S), \tag{2}$$

$$N_2(A\,{}^3\Sigma_u^+) + M \xrightarrow{k_{+3}^{(M)}} 2N({}^4S) + M, \tag{3}$$

$$N_2(A\,{}^3\Sigma_u^+) + M \underset{k_{-4}^{(M)}}{\overset{k_{+4}^{(M)}}{\rightleftharpoons}} N_2(B\,{}^3\Pi_g) + M, \tag{4}$$

$$N_2(B\,{}^3\Pi_g) \xrightarrow{\tau_5^{-1}} N_2(A\,{}^3\Sigma_u^+) + h\nu. \tag{5}$$

Apart from the inclusion of Reaction (3), the above set of reactions is the same as that previously proposed by Wray.[12] The over-all rate of the dissociation of ground-state N_2 behind shock waves has been measured

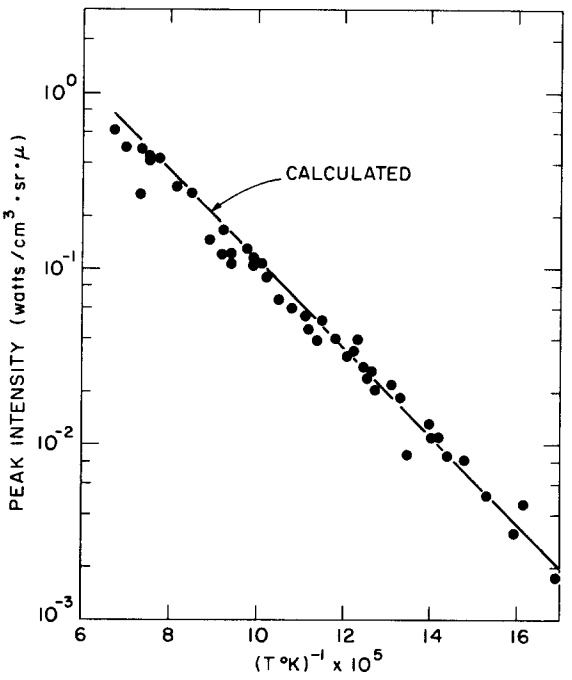

FIG. 3. Comparison of measured and calculated peak intensities of the $N_2(1+)$ emission. ●, Wray[13]; solid lines, this work.

over the temperature range 8000–15 000°K by Appleton, Steinberg, and Liquornik[18] for those cases where the collision partner M is either Ar, N_2, or N. Shui, Appleton, and Keck,[19] using the modified phase-space theory of reaction rates, have calculated the separate dissociation rate coefficients $k_{+1}^{(M)}$ and $k_{+3}^{(M)}$ for the case where the collision partner M is an argon atom. By assuming that the $N_2(A\,^3\Sigma_u^+)$ state was in local thermodynamic equilibrium with the ground state, they were able to match both the absolute magnitude and temperature dependence of the measured dissociation rate coefficients quite well using what appears to be a fairly realistic form for the two-body interatomic potential V_{ArN}. On the basis of the results to be described later, it appears that for the dissociation of N_2 diluted in an argon heat bath and at the temperatures of the shock-tube experiments, the assumption of local thermodynamic equilibrium is invalid. For the dissociation of pure N_2 at temperatures greater than about 8000°K, the $A\,^3\Sigma_u^+$ state concentration will also be shown later to be well below that calculated on the basis of local thermodynamic equilibrium during the rise time of $N_2(1+)$ radiation, and thus the dissociation of both undiluted N_2 and of diluted N_2 at high temperatures behind shock waves proceeds primarily via the ground state, i.e., Reaction (1). Therefore, the experimentally derived dissociation rate coefficient $k_D^{(M)}$ [18] has been used for $k_{+1}^{(M)}$, with the additional assumption that the ratio $k_{+3}^{(M)}/k_{+1}^{(M)}$ (M is N_2, Ar, N) is the same as that given by the phase-space theory calculations for M is Ar.[19] The ultimate justification for this assumption is provided by the results contained below; however, even on theoretical grounds this procedure should be anticipated to be approximately correct. [The phase-space theory[19] assumes that the three-body interaction potential is given by the sum of two-body potentials V_{N_2} and V_{NM}, where V_{N_2} is the ground-state ($X\,^1\Sigma_g^+$) molecular potential for the calculation of $k_{+1}^{(M)}$ and the first excited state ($A\,^3\Sigma_u^+$) molecular potential for the calculation of $k_{+3}^{(M)}$. V_{NM} is simply the interatomic potential between an $N(^4S)$ atom and the third body M; it is independent of the ultimate state of the combined atoms.]

In accord with Wray,[12] Reaction (4) was assumed to be sufficiently fast by comparison with any of the other reactions which serve to populate or depopulate either of the $N_2(A\,^3\Sigma_u^+)$ or $N_2(B\,^3\Pi_g)$ states that these two states may be assumed to be in local thermodynamic equilibrium with one another throughout the entire relaxation region. This assumption was subsequently justified by a numerical calculation using the derived estimate for $k_{+2}^{(N)}$, the measured radiative lifetime of the $B\,^3\Pi_g$ state[33] ($\tau_5 = 7\times10^{-6}$ sec), and an estimate of the collisional quenching rate coefficient $k_{-4}^{(M)} = 6.2\times10^{-11}$ cm³ sec⁻¹ obtained at $T = 300$°K.[34] The rate of the dissociation reaction,

$$N_2(B\,^3\Pi_g) + M \rightarrow N(^4S) + N(^2D) + M,$$

was shown theoretically[19] to be negligible by comparison with Reaction (3) due to its increased endothermicity.

B. Calculations and Comparison with Experiment: $N_2(1+)$

Using the above values for $k_{+1}^{(M)}$, $k_{+3}^{(M)}$, and τ_5 (see Table I for a summary of the individual rate coefficients used) and the assumption that the $A\,^3\Sigma_u^+$ and $B\,^3\Pi_g$ states were maintained in local thermodynamic equilibrium, the N-atom excitation rate coefficient, $k_{+2}^{(N)} = K_{e2}k_{-2}^{(N)}$, was deduced by matching computed $N_2(1+)$ emission profiles with those observed experimentally. The matching procedure used was as follows: The rise of the emission intensity behind the shock wave was calculated to the peak using a guessed estimate for the value of the rate coefficient $k_{-2}^{(N)}$. The computed maximum intensity was then compared with Wray's[13] absolute measured value. By iteration on the value of the rate coefficient $k_{-2}^{(N)}$, the calculated peak intensity was brought into agreement with the experimental value. This matching procedure was employed at several shock speeds which spanned the full experimental range of conditions. The empirical rate coefficients thus obtained were correlated by the following expression:

$$k_{-2}^{(N)} = 5.1\times10^{-3}T^{-2.23}\text{cm}^3\ \text{sec}^{-1} \qquad (3.1)$$

for the temperature range 6000°–14 000°K. Figure 3

TABLE I. Reaction rate coefficients used in calculation of radiation profiles.

Reaction	Rate coefficient[a]	Reference
(1) $N_2(X\,^1\Sigma_g^+)+M\rightarrow 2N(^4S)+M$	$k_{+1}^{(Ar)}=(2.3\pm0.2)\times10^{-3}T^{-1.6}\exp(-D^{(N_2)}/kT)$ $k_{+1}^{(N_2)}=(2.7\pm0.7)k_{+1}^{(Ar)}$; $k_{+1}^{(N)}=(12\pm4)k_{+1}^{(Ar)}$ $D^{(N_2)}/k=1.132\times10^5$ °K	18 18
(2) $N_2(A\,^3\Sigma_u^+)+N(^4S)\rightarrow N_2(X\,^1\Sigma_g^+)+N(^4S)$	$k_{-2}^{(N)}=5.1\times10^{-3}T^{-2.23}$	This work
(3) $2N(^4S)+M\rightarrow N_2(A\,^3\Sigma_u^+)+M$	$k_{-3}^{(M)}/k_{-1}^{(M)}=36T^{-0.36}$	19
(4) $N_2(A\,^3\Sigma_u^+)+M\rightleftharpoons N_2(B\,^3\Pi_g)+M$	Local equilibrium	...
(5) $N_2(B\,^3\Pi_g)\rightarrow N_2(A\,^3\Sigma_u^+)+h\nu$	$\tau_5=7.0\times10^{-6}$ (sec)	33
(6) $N_2^+(X\,^2\Sigma_g^+)+e^-\rightarrow 2N(^4S)$	$k_{-6}=(2.5\pm0.8)\times10^{-2}T^{-1.5}$	39
(7) $N_2^+(X\,^2\Sigma_g^+)+N(^4S)\rightleftharpoons N_2(X\,^1\Sigma_g^+)+N^+(^3P)$	Local equilibrium	...
(8) $N_2^+(X\,^2\Sigma_g^+)+M\rightleftharpoons N_2^+(A\,^2\Pi_u)+M$	Local equilibrium	...
(9) $N_2^+(B\,^2\Sigma_u^+)+N_2\rightarrow N_2^+(A\,^2\Pi_u)+N_2$ (10) $N_2^+(B\,^2\Sigma_u^+)+N_2\rightarrow N_2^+(X\,^2\Sigma_g^+)+N_2$	$k_q^{(N_2)}=(k_{-9}^{(N_2)}+k_{-10}^{(N_2)})=1.9\times10^{-2}T^{-2.33}$	This work
(11) $N_2^+(B\,^2\Sigma_u^+)\rightarrow N_2^+(X\,^2\Sigma_g^+)+h\nu$	$\tau_{11}=6.58\times10^{-8}$ (sec)	38

[a] Units: Species concentrations measured in particles per cubic centimeters, time in seconds, and temperature in degrees Kelvin.

shows the comparison of these calculated peak intensities with Wray's[13] measurements.

In Fig. 4 the values of $k_{-2}^{(N)}$ given by Eq. (3.1) are compared with those obtained by Wray[12] for the same temperature range, and with the room temperature rates determined by Young and St. John[35] and by Meyer, Setser, and Stedman.[36] It is apparent that the present estimate of $k_{-2}^{(N)}$ is more than an order of magnitude greater than Wray's estimate. The comparison shown in Fig. 3 will be discussed later in this paper.

Additional tests of the kinetic model, Reactions (1)–(5), and of the rate coefficients are provided by comparisons of the theoretically calculated times-to-peak intensity and the intensity profile shapes with the corresponding measurements; this information was not used in the matching procedure described above. Figure 5 presents a compilation of time-to-peak intensity data for the first-positive emission obtained in shock-tube experiments using undiluted N_2,[5,10,13] N_2/Ar,[7] and N_2/Ne[11] mixtures. It is apparent that the calculated values of τ_{pk} for pure nitrogen agree very well with the experimental data. Similar good agreement is observed for the N_2/Ar mixtures, although the recorded time was not the actual time to peak but rather a characteristic time, τ_{pk}', as shown in Fig. 6. Anticipating that the dissociation rate coefficients, $k_{+1}^{(Ne)}$ and $k_{+3}^{(Ne)}$, for neon as the collision partner do not differ greatly from the argon rate coefficients, $k_{+1}^{(Ar)}$ and $k_{+3}^{(Ar)}$, the actual times to peak calculated for the N_2/Ar mixtures have also been plotted for comparison with the measurements made in N_2/Ne mixtures. Again the agreement between theory and experiment appears to be satisfactory.

A representative emission intensity profile shape is presented in Fig. 6 for an observation made behind a shock wave in pure N_2. The shaded region represents the relative noise level of the oscilloscope trace, and the full line represents the theoretically calculated profile. The similarity between the theoretical and experimental profiles which extends well into the region where thermochemical equilibrium is approached, further substantiates the kinetic model and the rate coefficients used.

The calculated concentration history shown in Fig. 7 for a shock wave in undiluted N_2 is helpful to our understanding of the radiation overshoots of the first positive emission. Figure 7 corresponds to the radiation intensity profile of Fig. 6. The ground-state molecule concentration is observed to increase slightly with time due to the postshock density increase which is enhanced by shock-tube boundary layer development. The atom concentration remains small, reaching only 10% of the ground-state molecule concentration at times well after the peak intensity is achieved, although, of course, for stronger shock waves the degree of dissociation increases rapidly, becoming about 25% at the peak intensity for a postshock temperature of about 14 000°K.

The $A\,^3\Sigma^+$ state concentration at the intensity peak is about one-quarter of the local thermodynamic equilibrium value, which is represented by the dashed

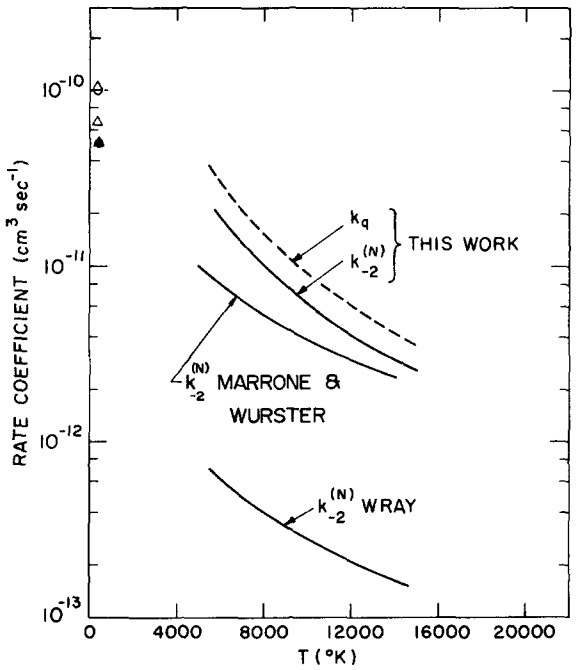

FIG. 4. Comparison of collisional quenching rates. $k_{-2}^{(N)}$: ●, Young and St. John[35]; ▲, Meyer, Setser, and Stedman[36]; solid lines, this work and Wray[12] and Marrone and Wurster[14] as indicated. $k_q^{(N_2)}$: ○, Brocklehurst[41]; △, Davidson and O'Neil[42]; dashed line, this work.

curve in Fig. 7. This difference increases with increasing temperature so that the $N_2(A\,^3\Sigma_u^+)$ concentration at peak intensity is less than one-tenth the equilibrium value at $T_2=14\,000°K$, whereas, at $T_2=6000°K$, it is greater than one-third of the equilibrium concentration. The reason for this relative behavior of the $A\,^3\Sigma_u^+$ concentration can be understood in terms of the expression which describes its steady-state variation. The steady-state $N_2(A\,^3\Sigma_u^+)$ concentration is achieved at about the time of the intensity maximum, and is given by

$$[N_2^*]=k_{+2}^{(N)}[N_2][N]/(k_{+3}^{(N_2)}[N_2]+k_{+3}^{(N)}[N]+k_{-2}^{(N)}[N]), \quad (3.2)$$

where $N_2^*=N_2(A\,^3\Sigma_u^+)$. Over much of the experimental temperature range, the term $k_{+3}^{(N_2)}[N_2]$ is the largest term in the denominator of Eq. (3.2), although the other terms are not wholly negligible, i.e., at $T=10\,000°K$, $k_3^{(N_2)}[N_2]/k_{-2}^{(N)}[N]=12$, and $k_{+3}^{(N_2)}[N_2]/k_{+3}^{(N)}[N]=2.3$. Thus, Eq. (3.2) may be only roughly approximated by

$$[N_2^*]=k_{+2}^{(N)}[N]/k_{+3}^{(N_2)}. \quad (3.3)$$

With the tacit assumption that during the intensity rise the N and N_2^* concentrations are populated according to the simplified rate equations,

$$d[N]/dt=2k_{+1}^{(N_2)}[N_2]^2 \quad (3.4)$$

and

$$d[N_2^*]/dt=k_{+2}^{(N)}[N_2][N], \quad (3.5)$$

and that the relaxation process is isothermal and the amount of dissociation is so small that the net rates of Reactions (1) and (2) remain constant, integration yields

$$[N]=2k_{+1}^{(N_2)}[N_2]^2t \quad (3.6)$$

and

$$[N_2^*]=k_{+2}^{(N)}k_{+1}^{(N_2)}[N_2]^3t^2. \quad (3.7)$$

It must be remembered that for pure nitrogen, particularly at high temperatures, the assumptions of constant N_2 concentration and temperature are valid only for times considerably shorter than the peak time. However, by approximating the population of N_2^* state by Eq. (3.7) until the steady-state concentration is reached, the important features of τ_{pk} become apparent. Combining this approximation with the steady-state concentration for N_2^* given by Eq.

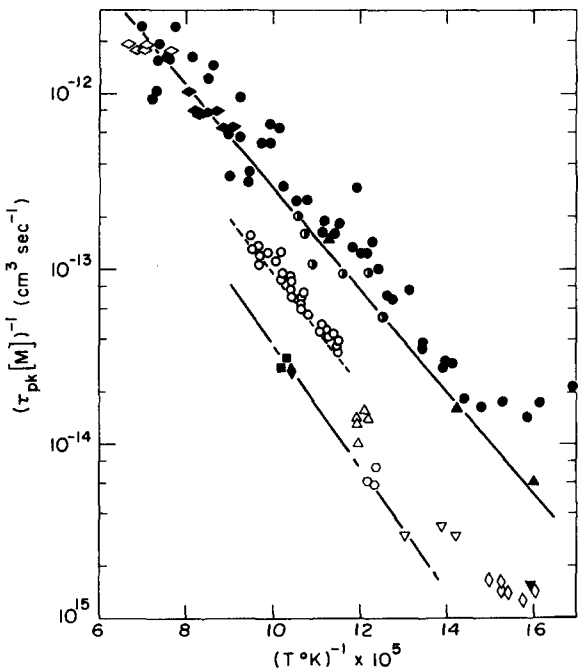

FIG. 5. Comparison of measured and calculated time-to-peak intensity of the first-positive system. Wray[13]: ●, 100% N_2, $P_1=1$ torr; Wurster and Marrone[10]: ▲, 100% N_2, $P_1=1$–5 torr; Keck, Camm, Kivel, and Wentink[5]: ◇, 100% N_2, $P_1=1$ torr; ◆, $P_1=3$ torr; ◑, $P_1=10$ torr; Smekhov and Losev[8]: ○, 10% N_2+90% Ar, $P_1=2$–10 torr; Marrone, Wurster, and Stratton[11]: ■, 10% N_2+90% Ne, $P_1=2$ torr; ◆, 7% N_2+93% Ne, $P_1=2$ torr; △, 3% N_2+97% Ne, $P_1=2$ torr; ◯, 3% N_2+97% Ne, $P_1=4$ torr; ▽, 0.5% N_2+99.5% Ne, $P_1=4$ torr; ◇, 3% N_2+97% Ne, $P_1=6$ torr; ▼, 0.5% N_2+99.5% Ne, $P_1=6$ torr. —, calculated τ_{pk}, 100% N_2, $P_1=1$ torr; - - -, calculated τ_{pk}', 10% N_2+90% Ar, $P_1=6$ torr; — - —, calculated τ_{pk}, 10% N_2+90% Ar, $P_1=6$ torr.

(3.3) yields

$$(\tau_{pk}[N_2])^{-1} \sim k_{+3}^{(N_2)}. \quad (3.8)$$

Similar approximations beyond the high-temperature extreme of the experimental data (at $T=15\,000°K$, $k_{+3}^{(N)}/k_{-2}^{(N)}>20$ and $k_{+3}^{(N)}[N]/k_{+3}^{(N_2)}[N_2]=1.9$) gives

$$(\tau_{pk}[N_2])^{-1} \sim (k_{+1}^{(N_2)} k_{+3}^{(N)})^{1/2}. \quad (3.9)$$

At low temperatures the steady-state concentration approaches local equilibrium, i.e., at $T=5000°K$, $k_{-2}^{(N)}[N]/k_{+3}^{(N_2)}[N_2]=1.4$ and $k_{-2}^{(N)}/k_{+3}^{(N)}=14$, so that

$$(\tau_{pk}[N_2])^{-1} \sim (k_{+1}^{(N_2)} k_{-2}^{(N)})^{1/2}. \quad (3.10)$$

Since the assumptions leading to Eqs. (3.6) and (3.7) are only approximations at best, one may only reasonably expect the observed times-to-peak intensity to be correlated by a plot of $\log[\tau_{pk}(N_2)^{-1}]$ vs T^{-1}, as suggested by the form of Eqs. (3.8)–(3.10). Indeed, this expectation appears to be fully realized by the results shown in Fig. 5. However, as indicated above, over most of the experimental temperature range, i.e., $T>6000°K$, the $N_2(A\ ^2\Sigma_u^+)$ concentration is much smaller than the corresponding equilibrium concentration, and thus the calculated times to peak are primarily determined by the dissociation Reactions (1) and (3) and are much less dependent on Reaction (2). Therefore, the good agreement between the calculated and measured times to peak as shown in Fig. 5 must reflect the essential accuracy of the values which were used for the dissociation rate coefficients $k_{+1}^{(M)}$ and $k_{+3}^{(M)}$ for M is N_2 and N.

The $N_2(A\ ^3\Sigma_u^+)$ state concentration for a dilute N_2/Ar mixture remains well below the corresponding equilibrium concentration even beyond the intensity maximum. A similar analysis as that outlined above for the steady-state concentration of the $A\ ^3\Sigma_u^+$ state shows that in the limit of a dilute mixture, it is approximately given by

$$[N_2^*]=k_{+2}^{(N)}[N_2][N]/k_{+3}^{(Ar)}[Ar] \quad (3.11)$$

over the experimental shock-tube temperature range. Equations similar to Eqs. (3.6) and (3.7) yield

$$(\tau_{pk}[Ar])^{-1} k_{+3}^{(Ar)}. \quad (3.12)$$

The same observation which was made for the case of undiluted N_2 is again valid, i.e., the good agreement between the calculated and measured times-to-peak intensity shown in Fig. 5 for dilute mixtures substantiate the essential accuracy of the value for $k_{+3}^{(Ar)}$ which was used in the calculations.

The accuracy of the rate coefficient $k_{-2}^{(N)}$ which was determined here is, of course, dependent on the validity of the assumed kinetic scheme, the accuracy of the other rate coefficients which were used, and the reliability of the flow model which has been used to take account of the shock-tube boundary layer effects. Exploratory calculations were carried out in which the values of the rates of Reactions (1) and (3) were altered by factors of 2. Calculations were also performed without making the boundary layer calculations. In this way the sensitivity of the derived values for $k_{-2}^{(N)}$ to the various assumptions was examined, and on this basis the expression for $k_{-2}^{(N)}$ [Eq. (3.1)] is estimated to be reliable to within a factor of about 2 over the temperature range 6000–14 000°K. In par-

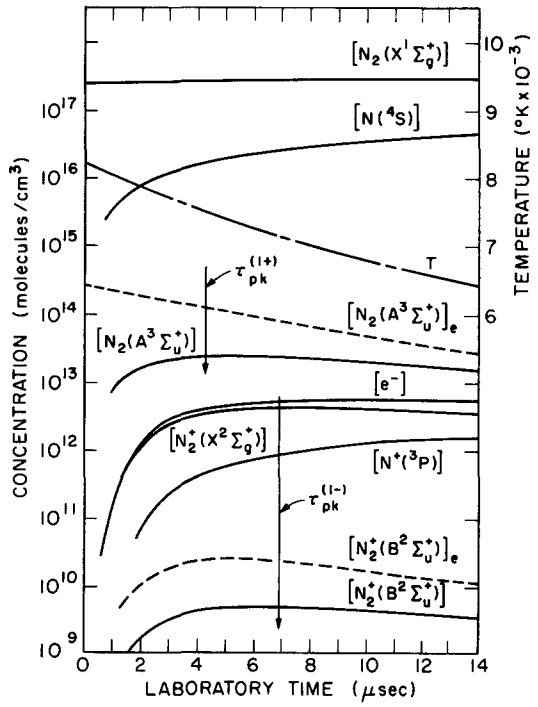

FIG. 7. Computed concentration histories. —, calculated; - - -, local thermodynamic equilibrium; — · —, temperature. Wray[12] profile: 100% N_2, $U_s=4.56$ mm/μsec, $P_1=1$ torr, $T_2=8210$ °K.

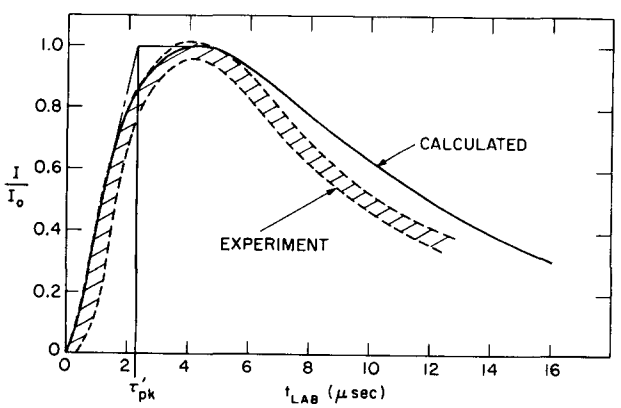

FIG. 6. Comparison of theoretically calculated $N_2(1+)$ emission profile (solid line) with experimental profile of Wray.[12] 100% N_2, $U_2=4.56$ mm/μsec, $P_1=1$ torr, $T_2=8210$ °K.

ticular, the boundary layer correction on the time-to-peak data obtained in Wray's small bore shock tube yielded an increase of the particle time at peak intensity of a factor of 1.3 at 14 000°K and increasing to a factor of 2 at about 7000°K. At lower temperatures where the intensity peak occurred near the contact surface, the effect of the boundary layer correction increased very rapidly, although it should be noted that this is likely to be a region where the quantitative boundary layer corrections become less well described by Mirel's theory.

Although there is no experimental evidence on which to base estimates of $k_{-2}^{(N)}$ within the temperature range 300–6000°K, it is clear from the results shown in Fig. 4 that a straight-line extrapolation would correlate both the room-temperature measurements and the shock-tube estimates of Eq. (3.1) quite well.

Before leaving the subject of the $N_2(1+)$ emission, two other reactions which have been suggested as being primary sources of the excited-state $N_2(A\ ^3\Sigma_u^+)$ will be briefly considered. The first reaction,

$$2N_2(X\ ^1\Sigma_g^+) \rightarrow N_2(A\ ^3\Sigma_u^+) + N_2(X\ ^1\Sigma_g^+), \qquad (2')$$

is spin forbidden, and although the N_2 ground state is by far the most abundant species immediately behind the shock waves, attempts to determine a rate coefficient for this reaction by the same matching procedures which allowed correlation of both the peak-intensity measurement and the time-to-peak intensity were unsuccessful. In addition, it is to be noted that Noxon[37] concluded from observations made in high-pressure nitrogen afterglow experiments that more than 10^9 collisions with ground-state molecules are required to effect electronic de-excitation of the $A\ ^3\Sigma_u^+$ state. Thus we believe that the above excitation reaction is too slow to be of importance in the shock wave experiments.

Smekhov and Losev[7] have suggested an alternative mechanism for the excitation of $N_2(A\ ^3\Sigma_u^+)$,

$$N_2(X\ ^1\Sigma_g^+) + e^- \underset{k_{-2^e}}{\overset{k_{+2^e}}{\rightleftharpoons}} N_2(A\ ^3\Sigma_u^+) + e^-, \qquad (2'')$$

where the electrons are generated by the associative ionization reaction to be discussed in the following section. Although the rate $k_{-2}^{(e)}$ may be much larger than $k_{-2}^{(N)}$, it is unlikely that the difference will be as great as the difference between the N and e^- concentrations except at very high temperatures. Using a recent estimate of the rate coefficient of Reaction $(2'')$,[38] i.e.,

$$k_{+2}^{(e)} = (5\pm 2)\times 10^{-5} T^{0.8} \exp(-80\,300/T)\ \text{cm}^3\ \text{sec}^{-1}$$

and calculated values for the concentrations and temperatures at the $N_2(1+)$ emission peaks, it was found that only as T_2 approaches 15 000°K does the contribution of Reaction $(2'')$ reach one-tenth of the rate of production of $N_2(A\ ^3\Sigma_u^+)$ by N_2+N collisions.

In an earlier study of the $N_2(1+)$ band system excitation mechanism, Marrone and Wurster[14] have performed similar computations to those described here. However, the dissociation of the $A\ ^3\Sigma_u^+$ state was not considered in this kinetic scheme, and the flow was considered to be inviscid. In spite of these differences, the rate coefficient which was deduced, $k_{-2}^{(N)} = 4.1\times 10^{-6} T^{-1.5}$ cm^3 sec^{-1}, is comparable to the value of the rate coefficient of Eq. (3.1) as is shown by the comparison in Fig. 4. Since the criteria used in Ref. 14 for comparing experimental and computed emission intensity profiles was the time to peak, a simplified analysis of the kinetic scheme, similar to that used in deriving Eqs. (3.8)–(3.10), shows the reasons for the agreement. With no dissociation of N_2* the steady-state concentration is the local equilibrium concentration, so that the same result as was found for the low-temperature extreme using the more complete kinetic scheme is obtained, i.e.,

$$[\tau_{pt}(N_2)]^{-1} \sim (k_{+1}^{(N_2)} k_{-2}^{(N)})^{1/2}. \qquad (3.10)$$

Thus, since the two will coincide at low temperatures, it is not surprising that the rate coefficient determined by Marrone and Wurster[14] is of the same magnitude as the value we deduce. It is to be noted, however, that the dissociation of $N_2(A\ ^3\Sigma_u^+)$ must be considered to accurately compute the absolute emission intensity.

C. Reaction Mechanism: $N_2^+(1-)$

The kinetic scheme which was found to best describe the shock-tube measurements of the $N_2^+(1-)$ system follows directly from that proposed by Hammerling, Teare, and Kivel[4]:

$$N(^4S) + N(^4S) \underset{k_{-6}}{\overset{k_{+6}}{\rightleftharpoons}} N_2^+(X\ ^2\Sigma_g^+) + e^-, \qquad (6)$$

$$N_2(X\ ^1\Sigma_g^+) + N^+(^3P) \underset{k_{-7}}{\overset{k_{+7}}{\rightleftharpoons}} N_2^+(X\ ^2\Sigma_g^+) + N(^4S), \qquad (7)$$

$$N_2^+(X\ ^2\Sigma_g^+) + M \underset{k_{-8}^{(M)}}{\overset{k_{+8}^{(M)}}{\rightleftharpoons}} N_2^+(A\ ^2\Pi_u) + M, \qquad (8)$$

$$N_2^+(A\ ^2\Pi_u) + M \underset{k_{-9}^{(M)}}{\overset{k_{+9}^{(M)}}{\rightleftharpoons}} N_2^+(B\ ^2\Sigma_u^+) + M, \qquad (9)$$

$$N_2^+(X\ ^2\Sigma_g^+) + M \underset{k_{-10}^{(M)}}{\overset{k_{+10}^{(M)}}{\rightleftharpoons}} N_2^+(B\ ^2\Sigma_u^+) + M, \qquad (10)$$

$$N_2^+(B\ ^2\Sigma_u^+) \xrightarrow{1/\tau_{11}} N_2^+(X\ ^2\Sigma_g^+) + h\nu. \qquad (11)$$

Dunn and Lordi[39] have recently estimated the associative ionization rate coefficient k_{-6} over the approximate temperature range 3500–7200°K from measurements of the electron density decay rate obtained

in a shock-tube wind tunnel nozzle. The expression which they give for k_{-6} was assumed to be valid at the higher temperatures which are of interest here.

Charge exchange cross sections of the type associated with Reaction (7) are known to be quite large, however, only crude estimates of the rate coefficients $k_{+7}=K_{e7}k_{-7}$ have been made; for example, Dunn and Lordi[39] suggest $k_{-7}=1.3\times10^{-13\pm1}T^{0.5}$ cm^3 sec^{-1}. An estimate of the rate coefficient for Reaction (8), i.e., $k_{-8}^{(N_2)}=10^{-9}$ cm^3 sec^{-1}, has been given by Bennett and Dalby[40] at $T=300°$K; it is anticipated that k_{-8} would not exhibit a significantly stronger temperature dependence than was observed for $k_{-2}^{(N)}$, see Fig. 4. Thus trial calculations were performed based on the estimates of k_{-7} and k_{-8} given above, and it was concluded that Reactions (7) and (8) would achieve local equilibrium well within the time required for the $N_2^+(1-)$ radiation to reach its intensity maximum over the experimental shock-tube temperature range.

To proceed further, not only were the $N_2^+(A\,^2\Pi_u)$ and $N^+(^3P)$ states assumed to be in local equilibrium with the ground states of the molecular ion, but in addition, it was assumed that the concentration of the $N_2^+(B\,^2\Sigma_u^+)$ state was given by the steady-state approximation at all times, i.e.,

$$[N_2^+(B\,^2\Sigma_u^+)]$$
$$=\frac{k_{+9}^{(M)}[N_2^+(A\,^2\Pi_u)][M]+k_{10}^{(M)}[N_2^+(X\,^2\Sigma_g^+)][M]}{k_{-9}^{(M)}[M]+k_{-10}^{(M)}[M]+\tau_{11}^{-1}}$$
$$=K_{e10}[N_2^+(X\,^2\Sigma_g^+)]\{k_q^{(M)}[M]/(k_q^{(M)}[M]+\tau_{11}^{-1})\}, \quad (3.13)$$

where the radiative lifetime of the $B\,^2\Sigma_u^+$ state is $\tau_{11}=6.58\times10^{-8}$ sec,[38] $K_{e10}[N_2^+(X\,^2\Sigma_g^+)]$ is the equilibrium concentration of the $B\,^2\Sigma_u^+$ state relative to the ground state of the ion, and $k_q^{(M)}=(k_{-9}^{(M)}+k_{-10}^{(M)})$ is the net collisional quenching rate of the $B\,^2\Sigma_u^+$ state to be determined.

D. Calculations and Comparison with Experiment: $N_2^+(1-)$

Radiation intensity profiles for the $N_2(1-)$ system were first computed for a range of conditions which spanned Wray's experimental shock-tube measurements. The dissociation kinetics of the N_2 were taken to be the same as those described previously, ionization was assumed to proceed via Reaction (6), Reactions (7) and (8) were assumed to be in local equilibrium, and the $N_2^+(B\,^2\Sigma_u^+)$ state concentration was assumed to be given by the steady-state condition, Eq. (3.13). By iteration on the value of $k_q^{(M)}$ at each temperature, it was a straightforward matter to match the calculated peak intensity with the absolute peak intensity measurements given by Wray.[13] In this way the following empirical expression for the net collisional quenching rate coefficient for the $B\,^2\Sigma^+$ state was deduced,

$$k_q^{(N_2)}=1.9\times10^{-2}T^{-2.33}\text{ cm}^3\text{ sec}^{-1}. \quad (3.14)$$

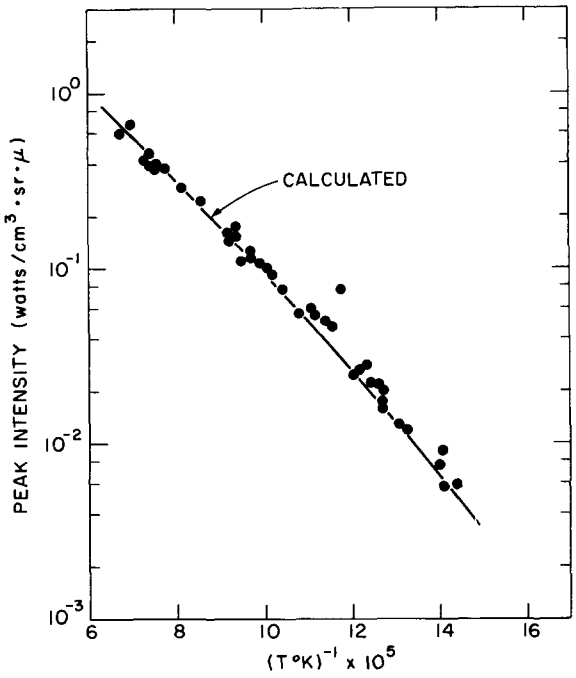

FIG. 8. Comparison of measured and calculated peak intensities of the $N_2^+(1-)$ emission. ●, Wray[13]; solid line, this work.

The calculated peak intensities are compared with Wray's measurements in Fig. 8, and a plot of $k_q^{(N_2)}$ [Eq. (3.14)] is shown in Fig. 4 together with the estimates of the low-temperature quenching rate coefficients determined by Brocklehurst[41] and Davidson and O'Neil[42] at $T=300°$K.

Figure 9 shows the comparison between measurements of the time required to reach the intensity maximum and our calculated estimates of these times. Since the $N_2^+(B\,^2\Sigma_u^+)$ state concentration was assumed to be given by the steady-state approximation, the calculated values of τ_{pk} are virtually independent of the rates of Reactions (8) and (9). Rather, the good agreement between the experimental and theoretical values of τ_{pk} shown in Fig. 9 reflect the essential accuracy of the dissociation rates and the high-temperature extrapolation of the rate for the associative ionization reaction, Reaction (6), used in the calculations. Also shown in Fig. 8 is the comparison between measurements of the characteristic time τ_{pk}' by Smekhov and Losev[7] (unfilled circles) for 10% N_2/Ar mixtures and computed values (dashed line) for which it was assumed that $k_q^{(Ar)}=k_q^{(N_2)}$. Again the comparison is seen to be quite good.

It is to be noted that the comparisons shown in Fig. 9 are effected by plotting $\log\{\tau_{pk}([N_2][M])^{1/2}\}^{-1}$ vs T^{-1} rather than $\log(\tau_{pk}[M])^{-1}$ versus T^{-1} as in Fig. 5 for the $N_2(1+)$ system. The reason for this method of comparison will now be examined.

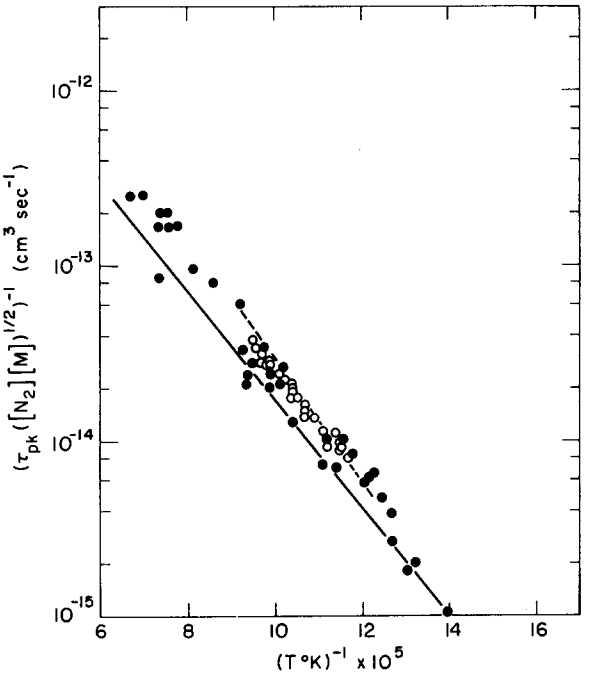

FIG. 9. Comparison of measured and calculated time-to-peak intensity of the first-negative system. Wray[13]: ●, 100% N_2, $P_1=1$ torr; Smekhov and Losev[7]: ○, 10% N_2+90% Ar, $P_1=1$–10 torr. Solid line: τ_{pk}, 100% N_2; dashed line: τ_{pk}', 10% N_2+90% Ar.

The species concentration profile illustrated in Fig. 7 shows that the dominant ionic species up to the time of the intensity maximum is the ground-state molecular ion. Furthermore, calculations have indicated that the peak intensity was achieved at about the time at which local equilibrium was approximately established for Reaction (6), i.e.,

$$[N_2^+(X\,^2\Sigma_g^+)]\simeq K_{e6}^{1/2}[N]. \tag{3.15}$$

By assuming that during the major portion of the period τ_{pk}, the N_2 concentration did not change significantly and that the conditions behind the shock wave were isothermal, the simplified rate equations,

$$d[N]/dt=k_{+1}^{(M)}[N_2][M] \tag{3.16}$$

and

$$d[N_2^+]/dt=k_{+6}[N]^2, \tag{3.17}$$

for $t<\tau$ are obtained; thus

$$[N_2^+]=4k_{+1}^{(M)2}k_{+6}[N_2]^2[M]t^3/3. \tag{3.18}$$

The further assumption that Eq. (3.18) is valid up to the point at which local equilibrium is approximately established for Reaction (6) gives

$$\{\tau_{pk}([N_2][M])^{1/2}\}^{-1}\sim(k_{+1}^{(M)}k_{-6}K_{e6}^{1/2})^{1/2}. \tag{3.19}$$

This approximate result explains why τ_{pk} is primarily determined by the dissociation kinetics of N_2 and the rate of the associative ionization reaction, as previously suggested, and the reason for the choice of the form for the ordinate in Fig. 9.

As observed for the case of the $N_2(1+)$ system, the reliability of the estimate for the collisional quenching rate of the $N_2^+(B\,^2\Sigma_u^+)$ state is dependent on the validity of the model reaction scheme and on the accuracy of the other rate coefficients used in the calculations. For this model reaction scheme, the various rates have been adjusted over their probable range of uncertainty to assess their relative importance in the over-all calculation, and on this basis the estimate of $k_q^{(M)}$ was observed to be accurate to within a factor of 2 or 3. Again, a linear extrapolation from the present high-temperature estimates of $k_q^{(M)}$ does appear to correlate with the low-temperature measurements shown in Fig. 4.

IV. CONCLUSIONS

The nonequilibrium radiation intensity profiles of the $N_2(1+)$ and $N_2^+(1-)$ band systems have been calculated using a computer program which allows calculations to be made of chemically reacting flows obtained behind normal shock waves produced in nonideal shock tubes. The model reaction schemes used in the computations followed directly from those proposed in earlier studies[4,12] and were found to yield good agreement with previously published[2–12] and unpublished[13] measurements of the absolute intensity, time-to-peak intensity, and intensity profile shapes.

Rate coefficients for the collisional quenching of the $N_2(A\,^3\Sigma_u^+)$ and $N_2^+(B\,^2\Sigma_u^+)$ states via the spin-allowed reactions,

$$N_2(A\,^3\Sigma_u^+)+N(^4S)\xrightarrow{k_q^{(N_2)}}N_2(X\,^1\Sigma_g^+)+N(^4S)$$

and

$$N_2^+(B\,^2\Sigma_u^+)+N_2\xrightarrow{k_q^{(N_2)}}N_2^+(A\,^2\Pi_u)$$
$$\text{or } N_2^+(X\,^2\Sigma_g^+)+N_2,$$

were deduced by matching the computed peak intensities with Wray's measurements and were found to be correlated by the empirical expressions,

$$k_{-2}^{(N)}=5.1\times10^{-3}T^{-2.23}\text{cm}^3\text{ sec}^{-1}$$

and

$$k_q^{(N_2)}=1.9\times10^{-2}T^{-2.33}\text{cm}^3\text{ sec}^{-1},$$

over the temperature range 6000–14 000°K. The rate coefficient $k_{-2}^{(N)}$ determined here is within a factor of 2 of Marrone and Wurster's estimate[14] while being approximately a factor of 10 greater than the value determined by Wray.[12] As previously noted, a linear extrapolation through the results shown in Fig. 4 would adequately correlate both the room-temperature measurements and the high-temperature estimates of $k_{-2}^{(N)}$ and $k_q^{(N_2)}$. The two rates so determined are observed to be of comparable magnitude, and both have a similar strong negative temperature depend-

ence. The reasons for this similarity are not clear, although it is to be noted from Fig. 4 that these high-temperature estimates of the rate coefficients extrapolate quite well to the corresponding low-temperature measurements.

No rate coefficients could be deduced for the spin-forbidden reaction,

$$N_2(X\,^1\Sigma_g^+)+N_2(X\,^1\Sigma_g^+)\rightarrow N_2(A\,^3\Sigma_u^+)+N_2(X\,^1\Sigma_g^+),$$

which were consistent with the experimental measurements of the $N_2(1+)$ emission profiles, and thus it was concluded that the rate of this reaction was much too slow by comparison with the spin-allowed N-atom excitation reaction to be important as an excitation mechanism.

The good agreement between the computed and measured time-to-peak intensity and the general profile shapes for both the $N_2(1+)$ and $N_2^+(1-)$ systems was observed to result from the choice of the rate coefficients which describe the dissociation kinetics of nitrogen[18,19] and of the ionization mechanism.[39] In particular, it appears that Shui, Appleton, and Keck's[19] estimate of the ratio $k_{-3}^{(M)}/k_{-1}^{(M)}$, is substantiated, although it is apparent that their assumption that $N_2(A\,^3\Sigma_u^+)$ and ground states are in local equilibrium is invalid for dissociation behind shock waves at temperatures greater than about 6000°K. Since the contribution of the $A\,^3\Sigma_u^+$ state to the net dissociation rate is smaller than they suggested, (less than 1% at 14 000°K and 34% at 6000°K) it explains the lack of an observed induction time in the nitrogen dissociation measurements.[43] Finally, as a consequence of the comparisons presented here for the $N_2^+(1-)$ system, it appears that Dunn and Lordi's[39] expression for the rate coefficient, k_{+6}, of the associative-ionization reaction can be extended up to 14 000°K.

* This research was supported by the Advanced Research Projects Agency of the Department of Defense and monitored by the Office of Naval Research under Contract No. N00014-67-A-0204-0040 and ARPA Order No. 322.

[1] F. R. Gilmore, J. Quant. Spectry. Radiative Transfer **5,** 369 (1965).
[2] R. A. Allen, J. C. Camm, and J. C. Keck, J. Quant. Spectry. Radiative Transfer **1,** 269 (1961).
[3] R. A. Allen, J. C. Keck, and J. C. Camm, Phys. Fluids **4,** 284 (1962).
[4] P. Hammerling, J. D. Teare, and B. Kivel, Phys. Fluids **2,** 422 (1959).
[5] J. C. Keck, J. C. Camm, B. Kivel, and T. Wentink, Jr., Ann. Phys. (N.Y.) **7,** 1 (1959).
[6] S. A. Losev and G. D. Smekhov, High Temperature **2,** 889 (1965).
[7] G. D. Smekhov and S. A. Losev, High Temperature **6,** 369 (1968).
[8] K. L. Wray and T. J. Connolly, J. Quant. Spectry. Radiative Transfer **5,** 111 (1965).
[9] R. A. Allen, J. Quant. Spectry. Radiative Transfer **5,** 511 (1965).
[10] W. H. Wurster and P. V. Marrone, J. Quant. Spectry. Radiative Transfer **7,** 591 (1967).
[11] P. V. Marrone, W. H. Wurster, and J. E. Stratton, "Shock-Tube Studies of N^+ and O^+ Recombination Radiation in the Vacuum Ultraviolet," Cornell Aero. Lab. Rept. AG-1729-A-7, June 1968.
[12] K. L. Wray, J. Chem. Phys. **44,** 623 (1966).
[13] We are grateful to Dr. K. L. Wray of Avco-Everett Research Lab for supplying us with his unpublished measurements of the time to reach peak intensity and the absolute maximum intensity.
[14] P. V. Marrone and W. H. Wurster, "Reentry Precursor Plasma Determination of the Vacuum Ultraviolet Photoionizing Radiation Flux," presented at Proceedings of the Fourth Plasma Sheath Symposium; The Entry Plasma Sheath and Its Effects on Space Vehicle Electromagnetic Systems, Vol. I. Held at NASA Langley Research Center, 13–15 October, 1970.
[15] I. M. Cambell and B. A. Thrush, Proc. Roy. Soc. (London) **A296,** 201 (1967).
[16] M. A. A. Clyne and D. H. Stedman, J. Chem. Phys. **49,** 425 (1968).
[17] F. Kaufman, Ann. Rev. Phys. Chem. **20,** 45 (1969).
[18] J. P. Appleton, M. Steinberg, and D. J. Liquornik, J. Chem. Phys. **48,** 599 (1968).
[19] V. H. Shui, J. P. Appleton, and J. C. Keck, J. Chem. Phys. **53,** 2547 (1970).
[20] R. C. Millikan and D. R. White, J. Chem. Phys. **39,** 3209 (1963).
[21] J. P. Appleton, J. Chem. Phys. **47,** 3231 (1967).
[22] C. A. Brau, J. C. Keck, and G. F. Carrier, Phys. Fluids **9,** 1885 (1966).
[23] R. E. Duff, Phys. Fluids **2,** 207 (1959).
[24] A. Roshko, Phys. Fluids **3,** 835 (1960).
[25] W. J. Hooker, Phys. Fluids **4,** 1451 (1961).
[26] H. Mirels, Phys. Fluids **6,** 1201 (1963).
[27] P. J. Musgrove and J. P. Appleton, Appl. Sci. Res. **18,** 116 (1967).
[28] H. Mirels, Phys. Fluids **9,** 1265 (1966).
[29] H. Mirels, Phys. Fluids **9,** 1907 (1966).
[30] R. C. Flagan and J. P. Appleton, "The Excitation Mechanism of the Nitrogen First Position and First Negative Radiation at High Temperature," M.I.T. Fluid Mech. Rept. No. 71-7, April 1971.
[31] W. H. Wurster, "Measured Transition Probability for the First-Positive Band System," Cornell Aero. Labs. Rept. No. QM-1626-A-3, January 1962.
[32] D. E. Buttrey and H. R. McChesney, "Analysis of Emission Intensity Data for Shock-Heated N_2, O_2, NO, and Air," Air Force Weapons Laboratory Tech. Rept. No. AFWL-TR-69-29, December 1969.
[33] M. Jeunehomme, J. Chem. Phys. **45,** 1805 (1966).
[34] W. Brennan and E. C. Shane, Chem. Phys. Letters **2,** 143 (1968).
[35] R. A. Young and G. A. St. John, J. Chem. Phys. **48,** 895 (1968).
[36] J. A. Meyer, D. W. Setser, and D. H. Stedman, J. Phys. Chem. **74,** 2238 (1970).
[37] J. F. Noxon, J. Chem. Phys. **36,** 926 (1962).
[38] F. R. Gilmore, E. Bauer, and J. W. McGowan, J. Quant. Spectry. Radiative Transfer **9,** 157 (1969).
[39] M. G. Dunn and J. A. Lordi, "Measurement of $N_2^+ + e^-$ Dissociative Recombination in Expanding Nitrogen Flows," Cornell Aero. Lab. Rept. AI-2187-A-13, April 1969.
[40] R. G. Bennet and F. W. Dalby, J. Chem. Phys. **31,** 435 (1959).
[41] B. Brocklehurst, Trans. Faraday Soc. **60,** 2151 (1964).
[42] G. Davidson and R. O'Neil, J. Chem. Phys. **41,** 3946 (1964).
[43] J. P. Appleton, M. Steinberg, and D. J. Liquornik, J. Chem. Phys. **52,** 2205 (1970).